Supporting Information

AIE-Active Cyclometalated Iridium(III) Complexes for Detection of Lipopolysaccharide and Wash-Free Imaging of Bacteria

Aryan Gautam,[1] Ajay Gupta,[1] Puja Prasad,[2] and Pijus K. Sasmal[1]*

[1]School of Physical Sciences, Jawaharlal Nehru University, New Delhi 110067, India
[2]Amity Institute of Click Chemistry Research and Studies, Amity University, Noida, Uttar Pradesh 201303, India

**corresponding author: pijus@mail.jnu.ac.in*

Table of Contents

1. **Materials**
2. **Instruments**
   - 2.1 Thin layer chromatography and column chromatography
   - 2.2 NMR spectroscopy
   - 2.3 Mass spectrometry
   - 2.4 FT-IR spectroscopy
   - 2.5 UV-vis spectroscopy
   - 2.6 Emission spectroscopy
   - 2.7 Dynamic light scattering (DLS)
   - 2.8 Transmission electron microscopy (TEM)

Supplementary Table

Table S1. The LOD of the complexes (**Ir1-Ir3**) towards LPS.

Supplementary Figures

Figures S1-S2. ^{1}H and ^{13}C NMR spectra of compound **2** in DMSO-d_6.

Figures S3-S4. ^{1}H and ^{13}C NMR spectra of compound **3** in $CDCl_3$.

Figures S5-S6. ^{1}H and ^{13}C NMR spectra of compound **4** in $CDCl_3$.

Figures S7-S8. ^{1}H and ^{13}C NMR spectra of compound **L** in $CDCl_3$.

Figure S9-S10. ^{1}H NMR and ^{13}C NMR spectra of **Ir1** in $CDCl_3$.

Figures S11-S12. ^{1}H NMR and ^{13}C NMR spectra of **Ir2** in $CDCl_3$.

Figures S13-S14. ^{1}H NMR and ^{13}C NMR spectra of **Ir3** in $CDCl_3$.

Figure S15. ESI-HRMS of compound **2**.

Figure S16. ESI-HRMS of compound **L**.

Figures S17-S19. ESI-HRMS of the complexes **(Ir1-Ir3)**.

Figure S20. Absorption and emission spectra of complexes (**Ir1-Ir3**).

Figure S21. Emission spectra of **Ir2** in a water-THF mixture with different THF fractions.

Figure S22-S24. Size distribution of complexes (**Ir1-Ir3**) in a water-THF mixture with different THF fractions.

Figure S25. Emission intensity of complex **Ir1** as a function of concentration.

Figure S26-S28. Phosphorescence titration spectra of the complexes (**Ir1-Ir3**) upon addition of LPS.

Figure S29. Size distribution of **Ir1** in the absence and presence of LPS.

Figure S30. TEM images of **Ir1** in the absence and presence of LPS.

Figure S31. Effect of pH on the emission intensity of **Ir2** in the presence and absence of LPS.

Figure S32. Bacterial agglutination test in spiked water samples visualized by optical microscopy.

2. Instruments

2.1 Thin layer chromatography (TLC) and column chromatography

TLC was performed on aluminium plates coated with silica gel mixed with fluorescent indicator. The purification of synthesized ligand and complexes were performed with silica gel (60-120 mesh) column chromatography.

2.2 NMR spectroscopy

^{1}H and ^{13}C NMR spectra were acquired on a Bruker 400 and 500 MHz spectrometer in $CDCl_3$ or DMSO-d_6 at ambient temperature with tetramethylsilane (TMS) as an internal standard. NMR standards used were as follows: (^{1}H-NMR) $CDCl_3$ = 7.260 ppm; DMSO-d_6 = 2.50 ppm. (^{13}C-NMR) $CDCl_3$ = 77.16 ppm; DMSO-d_6 = 39.52 ppm. All chemical shifts (δ) are reported in ppm relative to TMS. Spin multiplicities were reported as a singlet (s), doublet (d), triplet (t), quartet (q), doublet of doublets (dd), triplet of doublets (td), multiplet (m) and broad (br) with coupling constant (J) reported in Hz.

2.3 Mass spectrometry

Electrospray ionization mass spectrometry (ESI-MS) and high-resolution mass spectrometry (ESI-HRMS) were recorded on Xevo G2-XS QTof Quadrupole Time of Flight Mass Spectrometer from Waters India Pvt. Ltd.

2.4 FT-IR spectroscopy

Fourier transform-Infrared (FT-IR) spectra were measured using IR Affinity-1S (Shimadzu, Kyoto, Japan) FT-IR spectrophotometer equipped with a single reflection attenuated total reflectance (ATR) accessory. The IR spectra were recorded from 4000 to 450 cm^{-1} using a resolution of 4 cm^{-1} with 45 scans. In IR absorption spectra, the shapes and signal intensities (height) of peaks (bands) are denoted by the following abbreviations: br = broad, vs = very strong, s = strong, m = medium and w = weak.

2.5 UV-vis spectroscopy

UV-vis absorption spectra were measured using a SpectraMax M2 plate reader (Molecular Devices) and an Agilent Technologies Carry 100 spectrophotometer, respectively, at 298 K from 800 to 200 nm.

2.6 Emission spectroscopy

Emission spectra and quantum yields were carried out on Edinburgh Instruments F900 fluorescence spectrophotometer.

2.7 Dynamic light scattering (DLS)

DLS was carried out using Zetasizer Nano ZS90 (Malvern Instrument Ltd., Worcestershire, UK).

2.8 Transmission electron microscopy (TEM)

Transmission electron microscopy images were taken on a JEOL JEM-1400 electron microscope operated at an acceleration voltage of 120 kV.

Table S1 The LOD of LPS by the complexes (**Ir1-Ir3**) determined using fluorescence spectroscopy.

Complexes	LOD (nM)
Ir1	47 ± 5
Ir2	144 ± 8
Ir3	157 ± 5

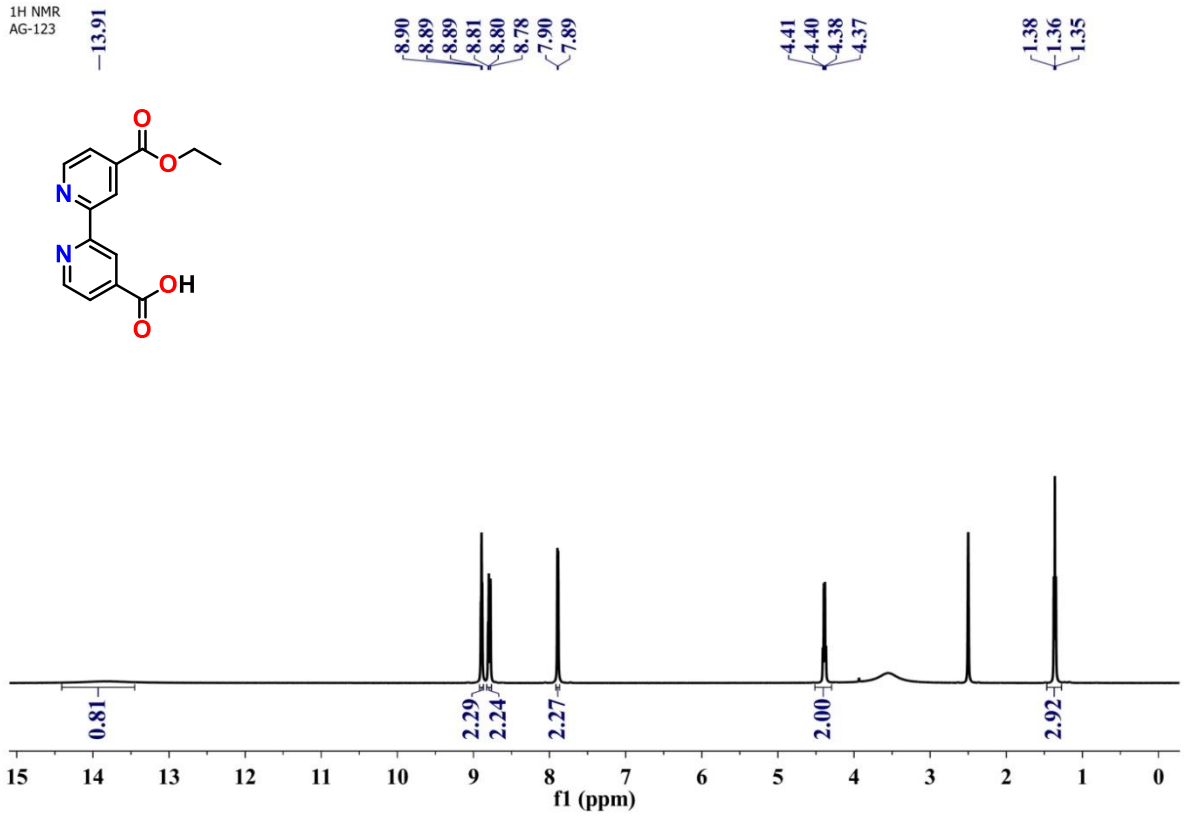

Figure S1 ^{1}H-NMR spectrum of compound **2** in DMSO-d_6 at 298K.

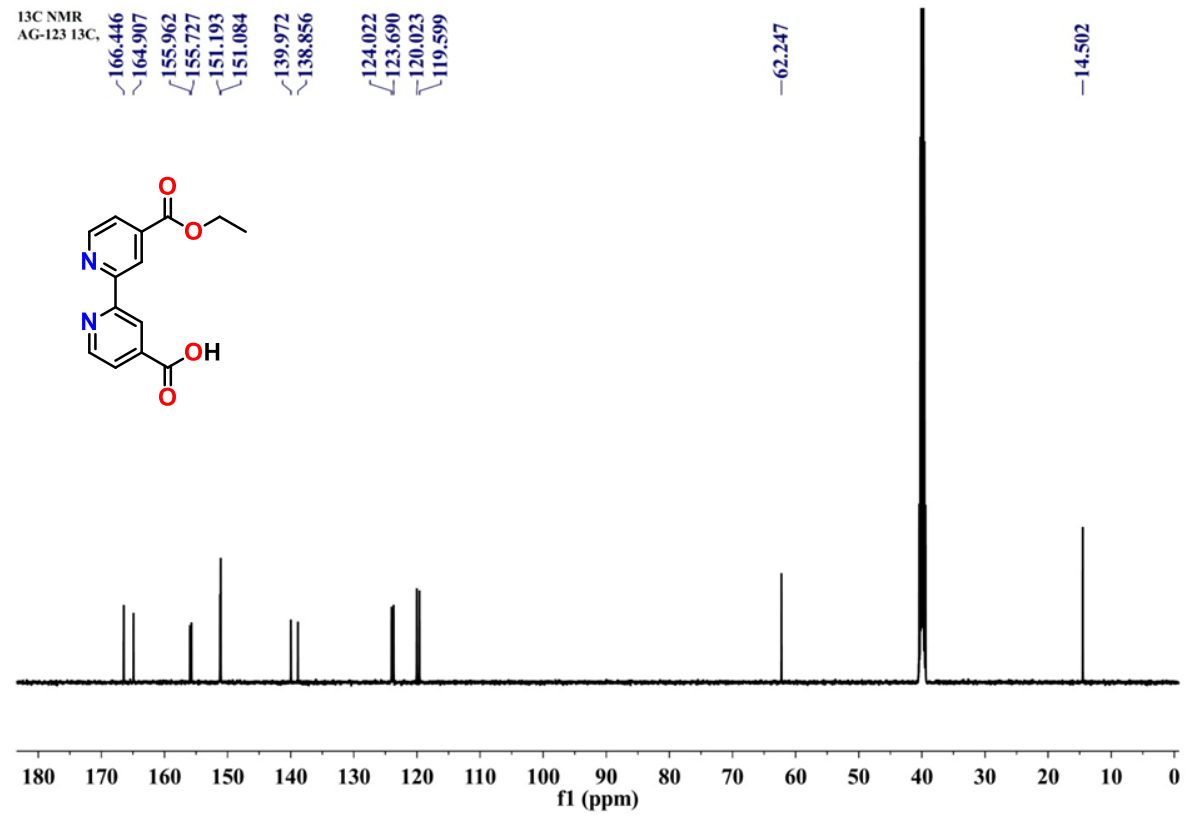

Figure S2 ^{13}C-NMR spectrum of compound **2** in DMSO-d_6 at 298K.

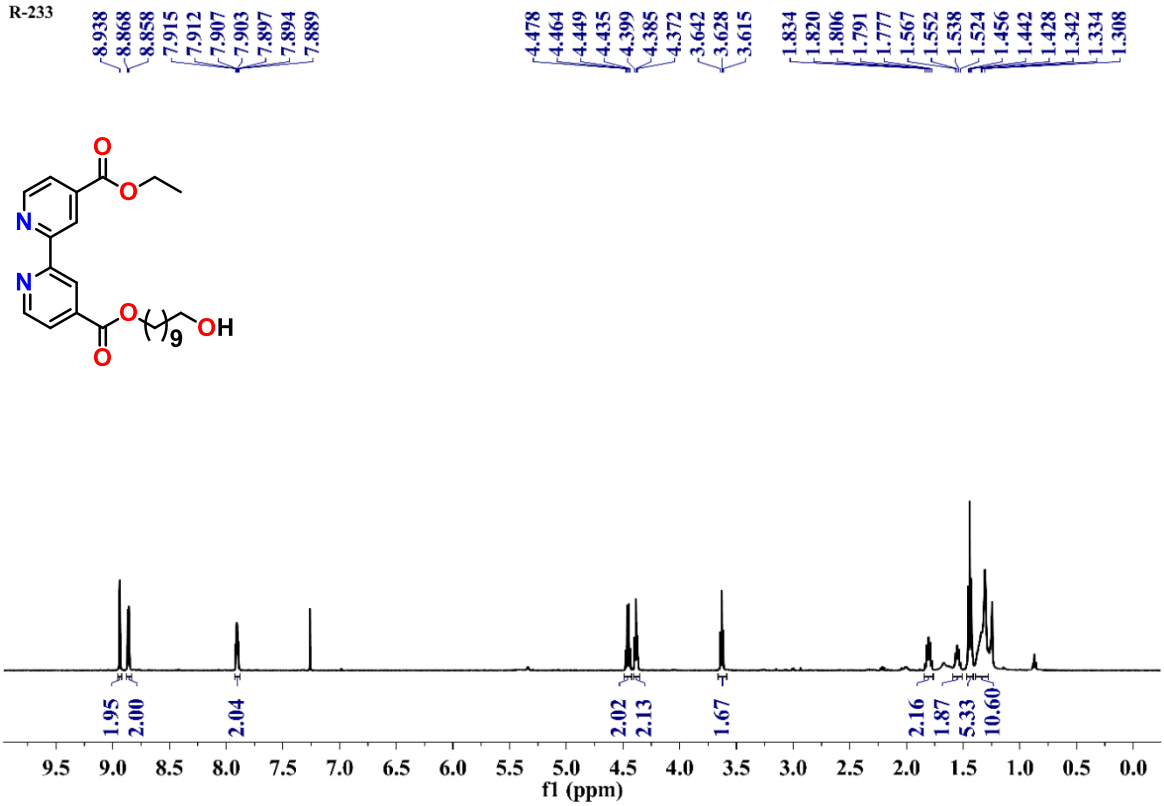

Figure S3 ^{1}H-NMR spectrum of compound **3** in $CDCl_3$ at 298K.

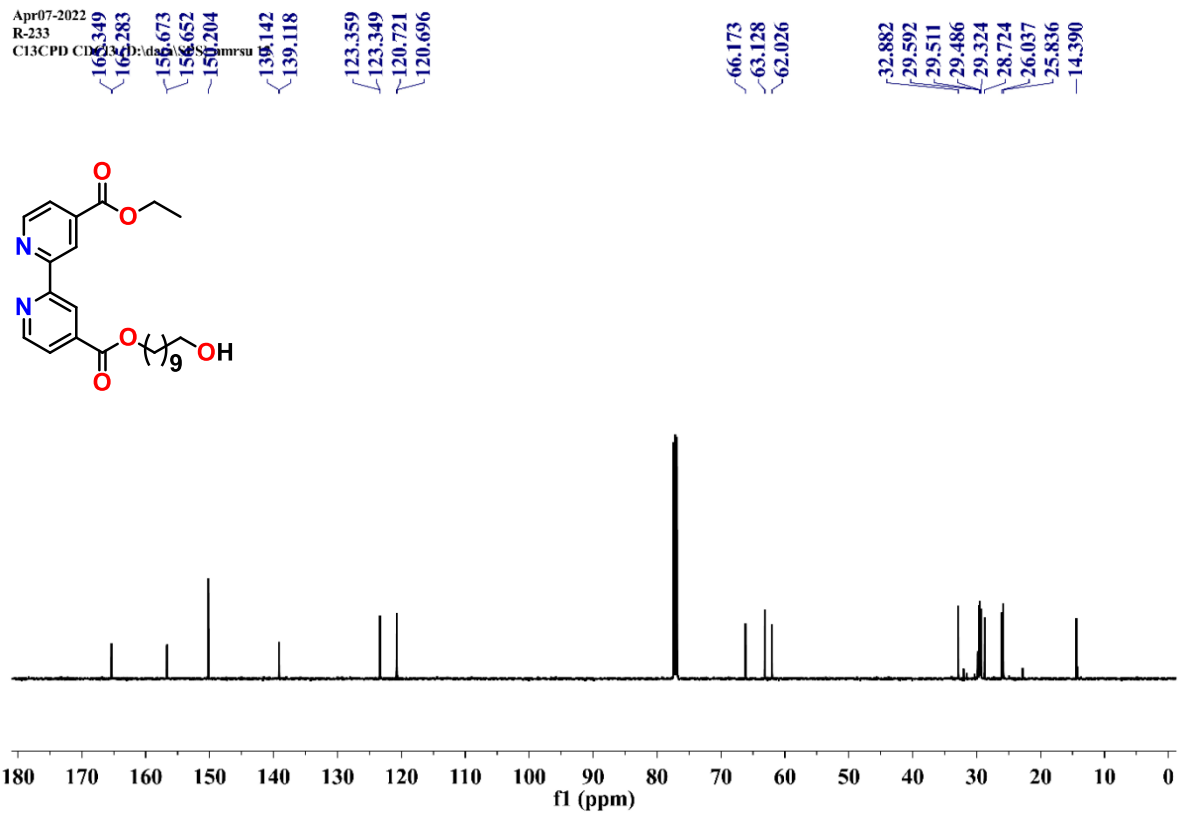

Figure S4 ^{13}C-NMR spectrum of compound **3** in $CDCl_3$ at 298K.

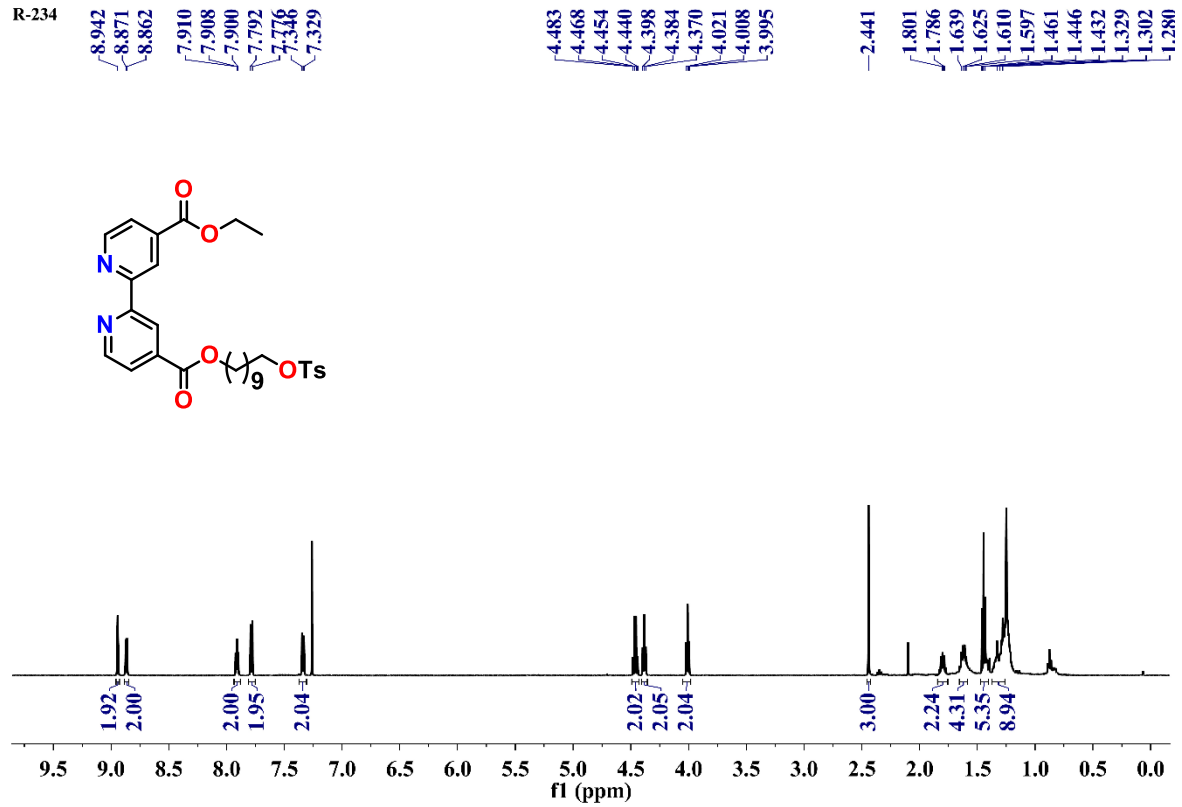

Figure S5 ^{1}H-NMR spectrum of compound **4** in $CDCl_3$ at 298K.

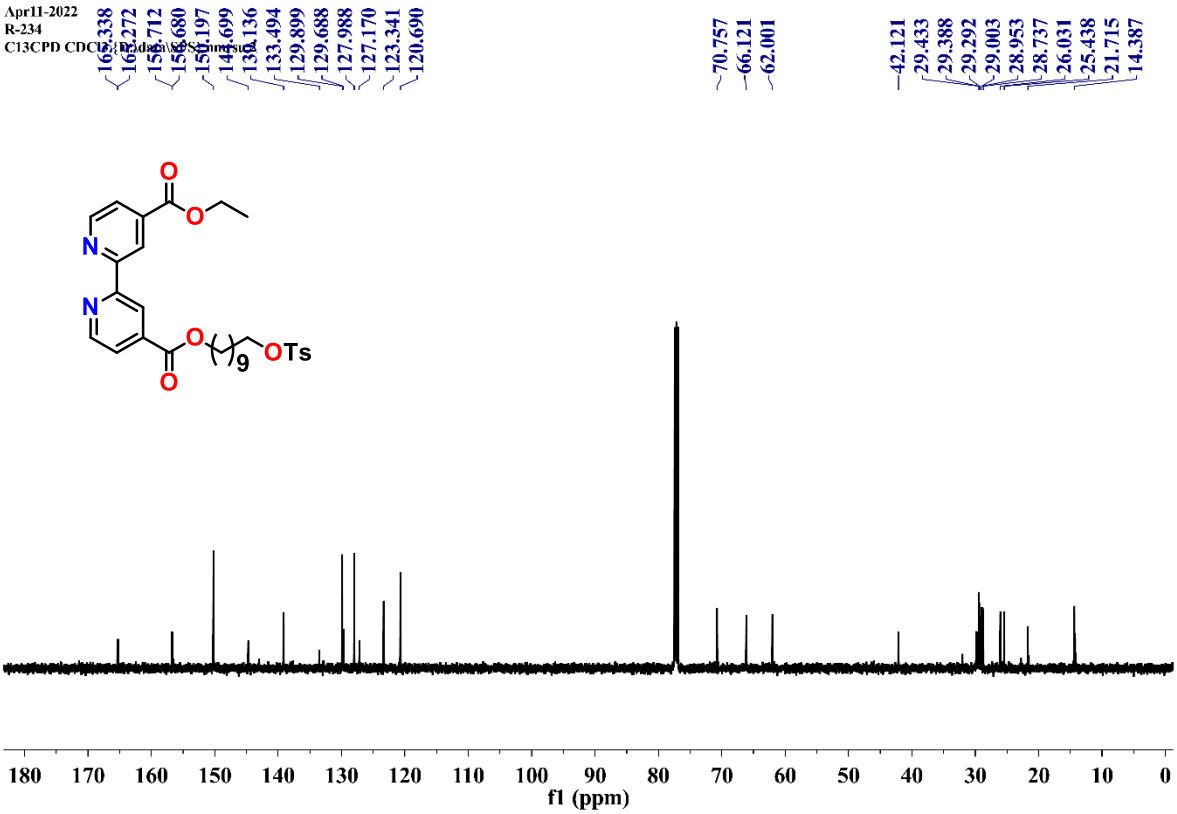

Figure S6 ^{13}C-NMR spectrum of compound **4** in $CDCl_3$ at 298K.

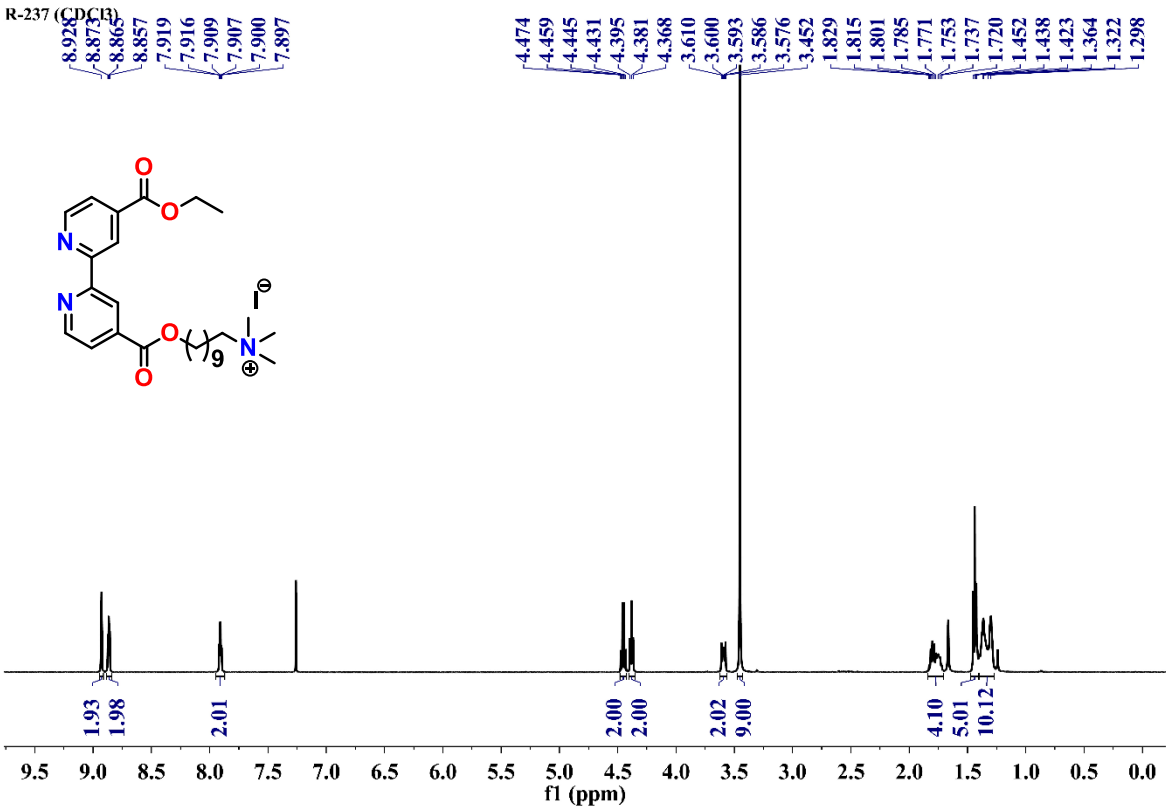

Figure S7 ^{1}H-NMR spectrum of compound **L** in $CDCl_3$ at 298K.

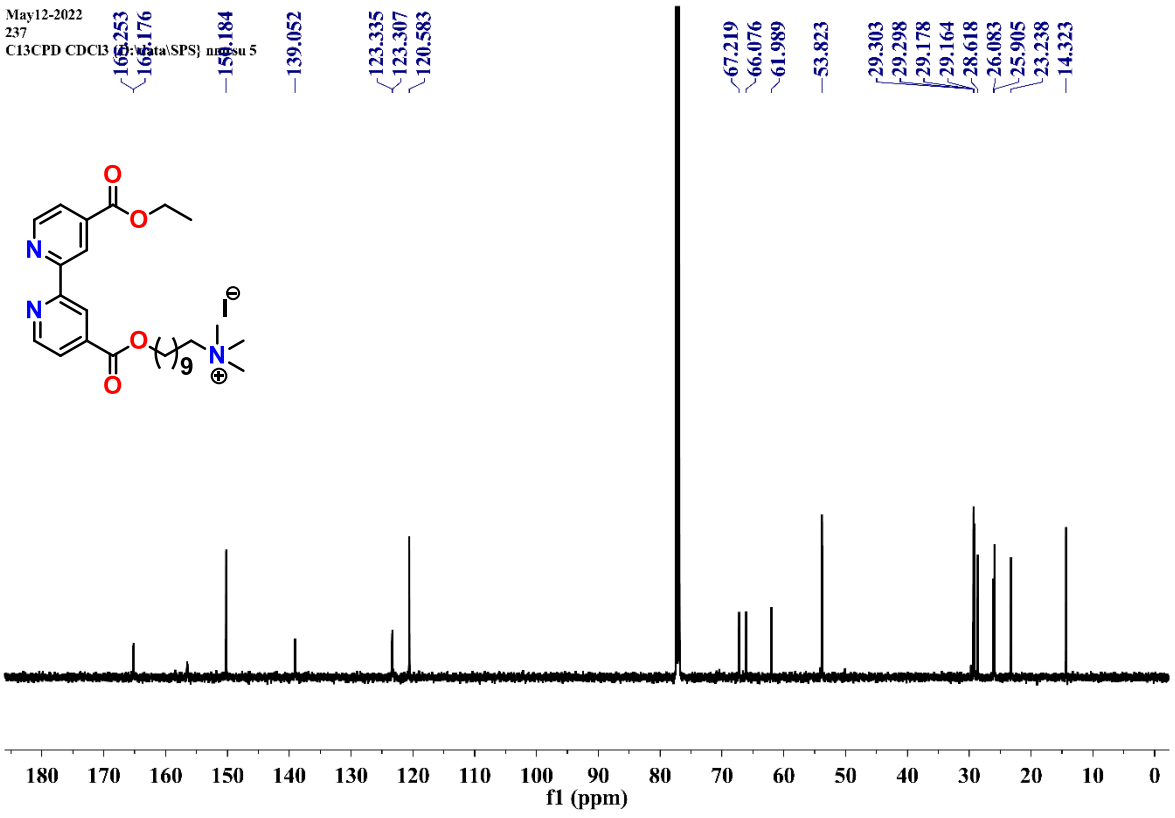

Figure S8 ^{13}C-NMR spectrum of compound **L** in $CDCl_3$ at 298K.

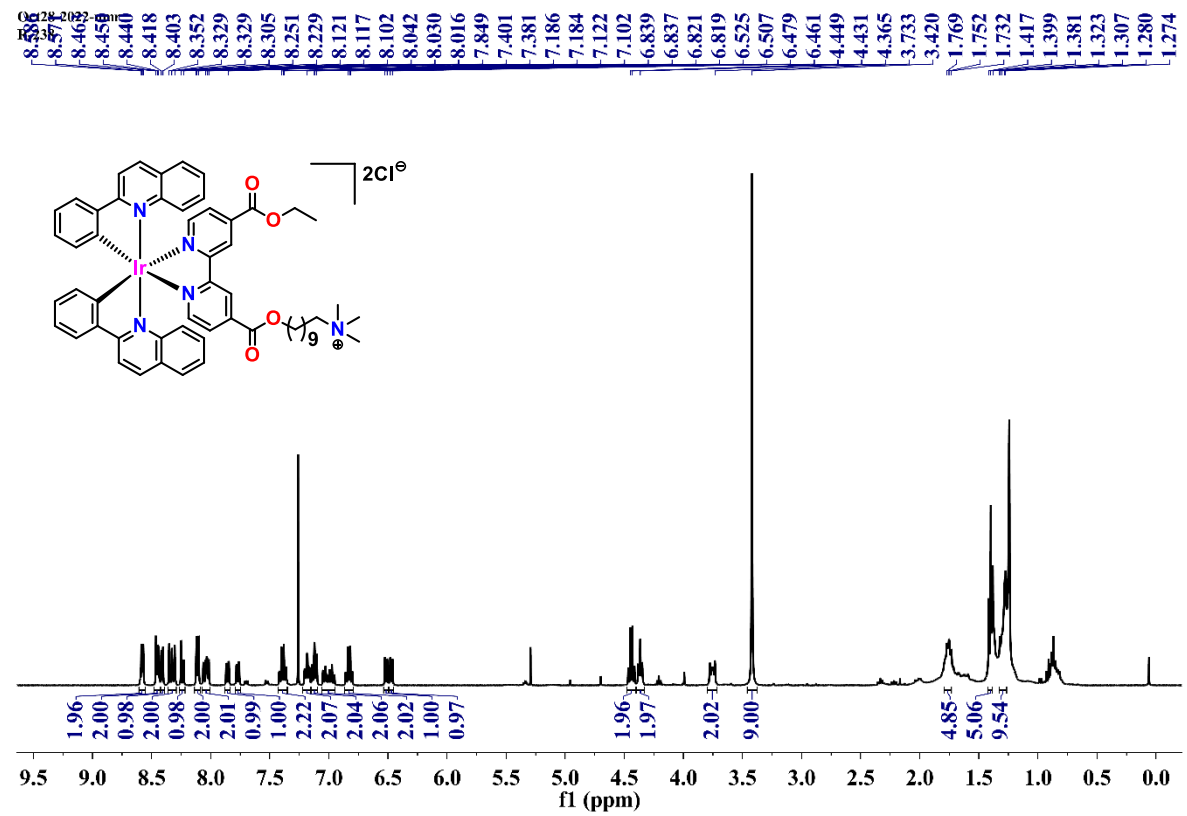

Figure S9 ^{1}H-NMR spectrum of **Ir1** in $CDCl_3$ at 298K.

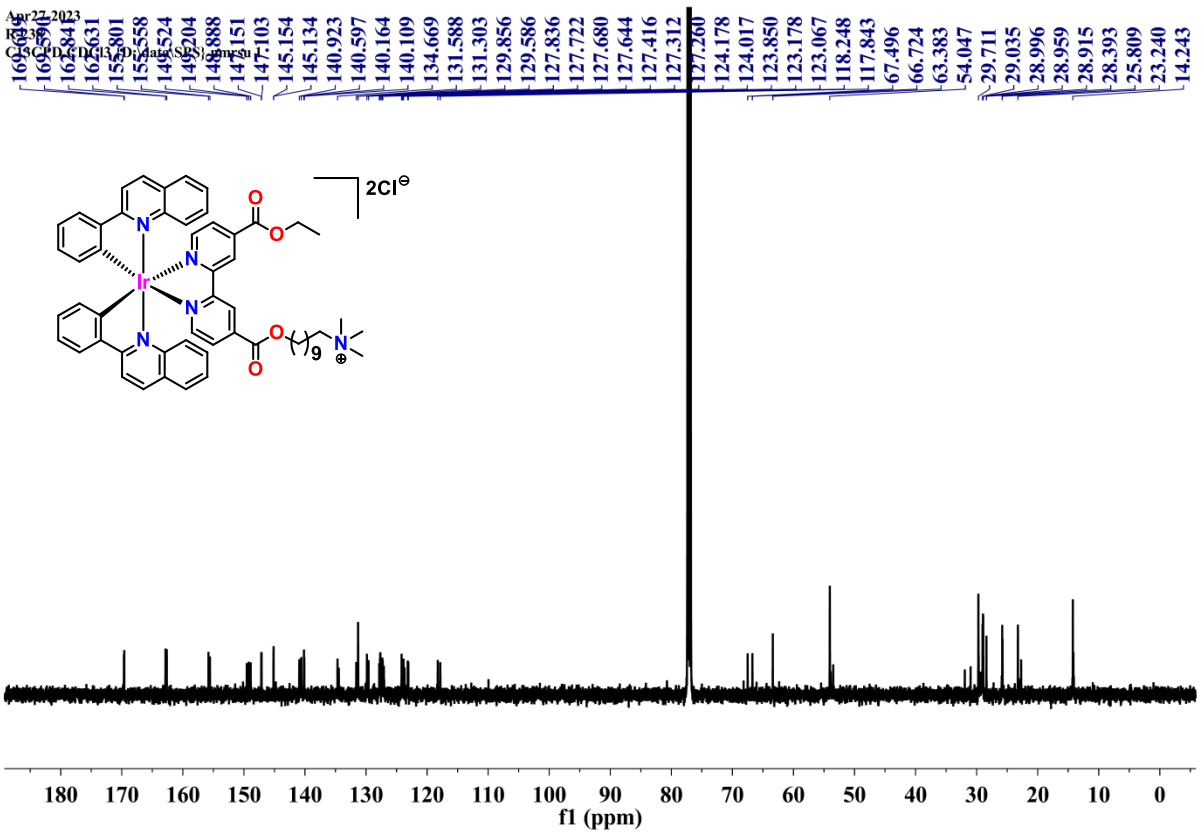

Figure S10 ^{13}C-NMR spectrum of **Ir1** in $CDCl_3$ at 298K.

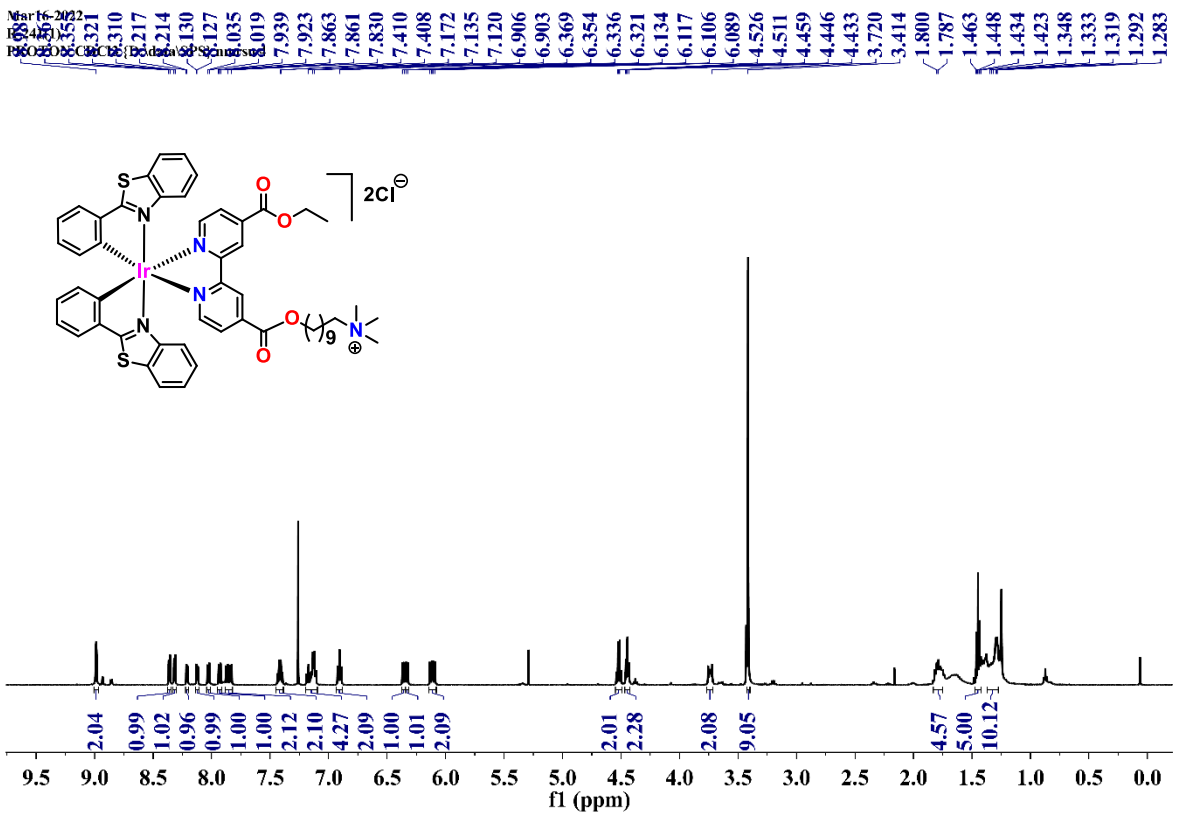

Figure S11 ^{1}H-NMR spectrum of **Ir2** in $CDCl_3$ at 298K.

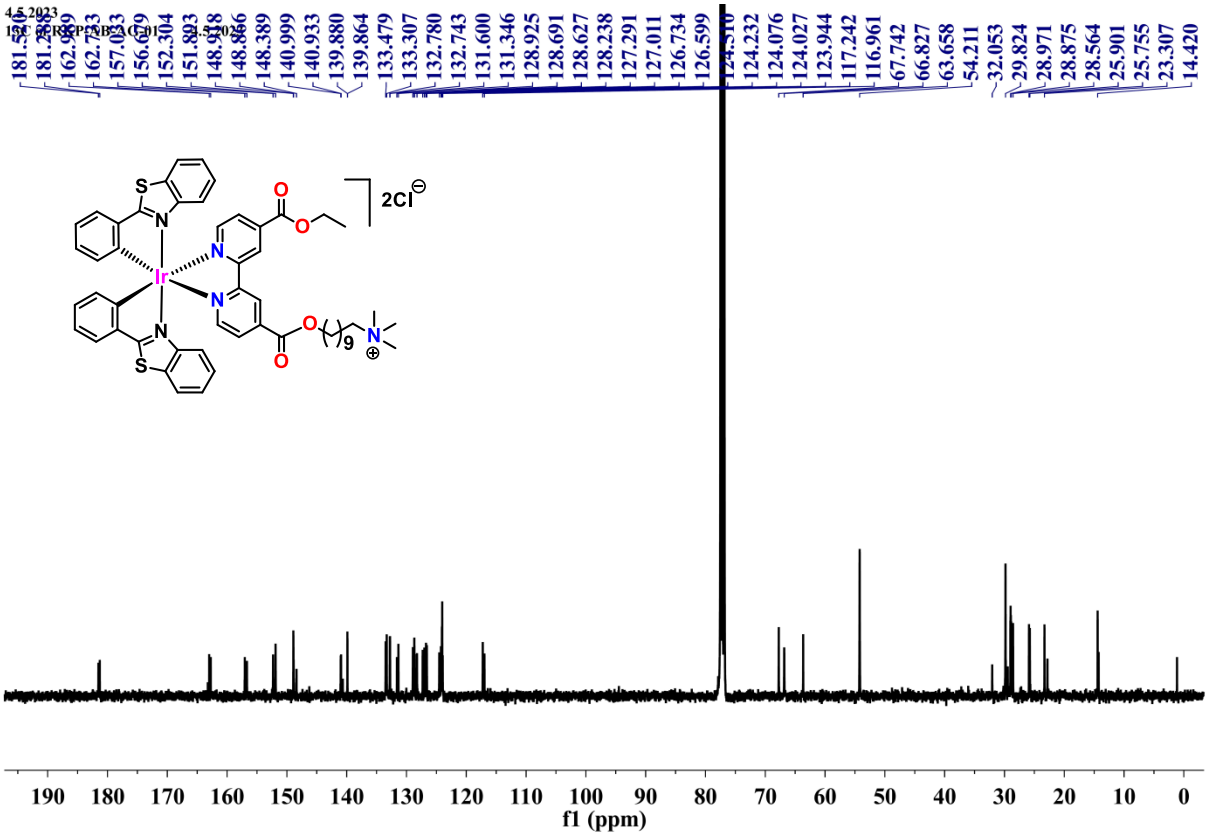

Figure S12 ^{13}C-NMR spectrum of **Ir2** in $CDCl_3$ at 298K.

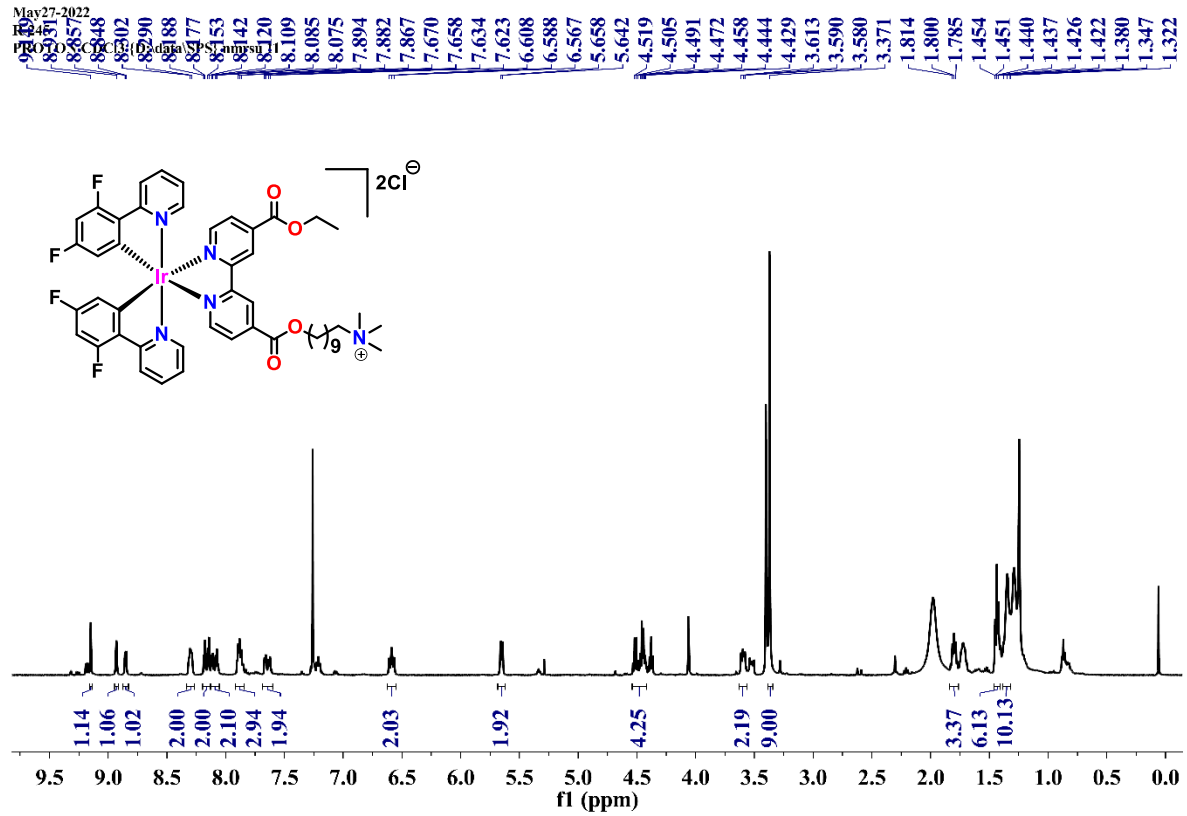

Figure S13 ^{1}H-NMR spectrum of **Ir3** in $CDCl_3$ at 298K.

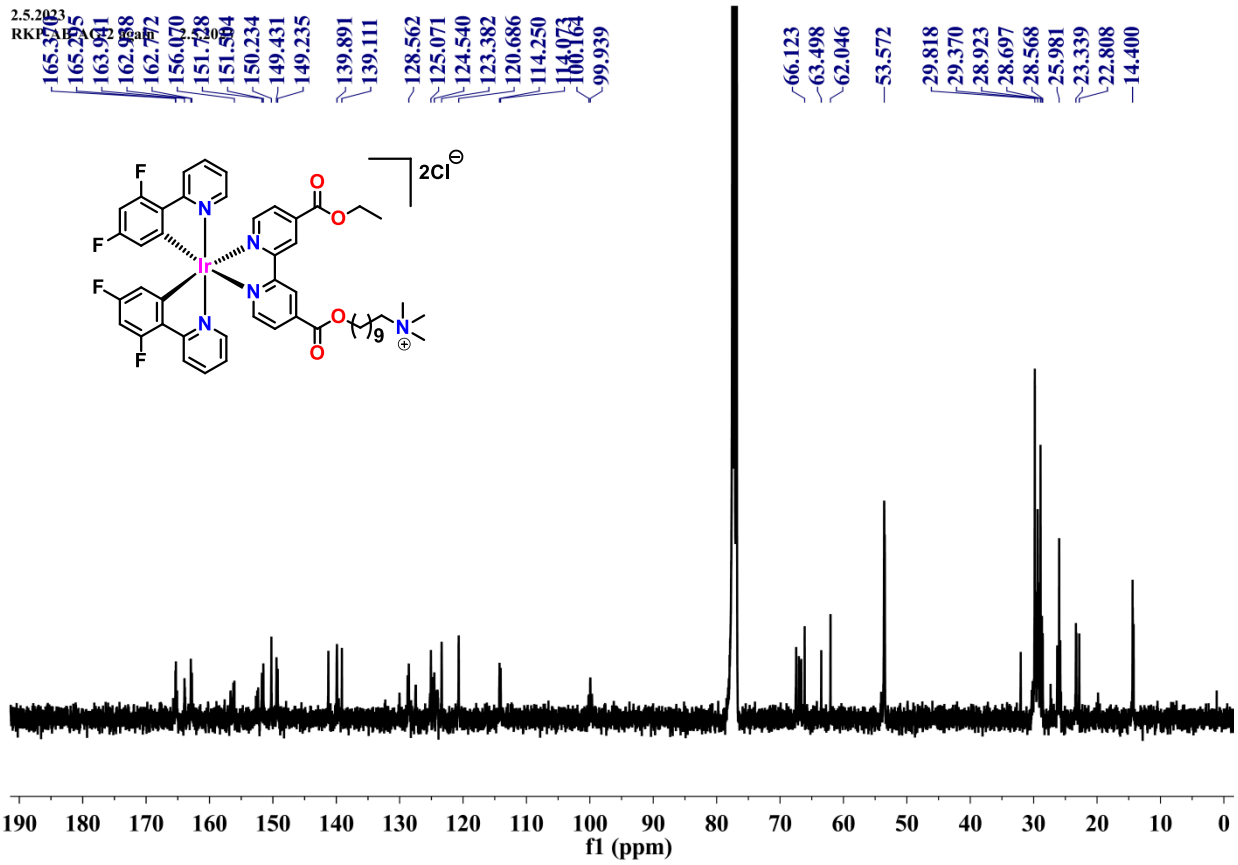

Figure S14 ^{13}C-NMR spectrum of **Ir3** in $CDCl_3$ at 298K.

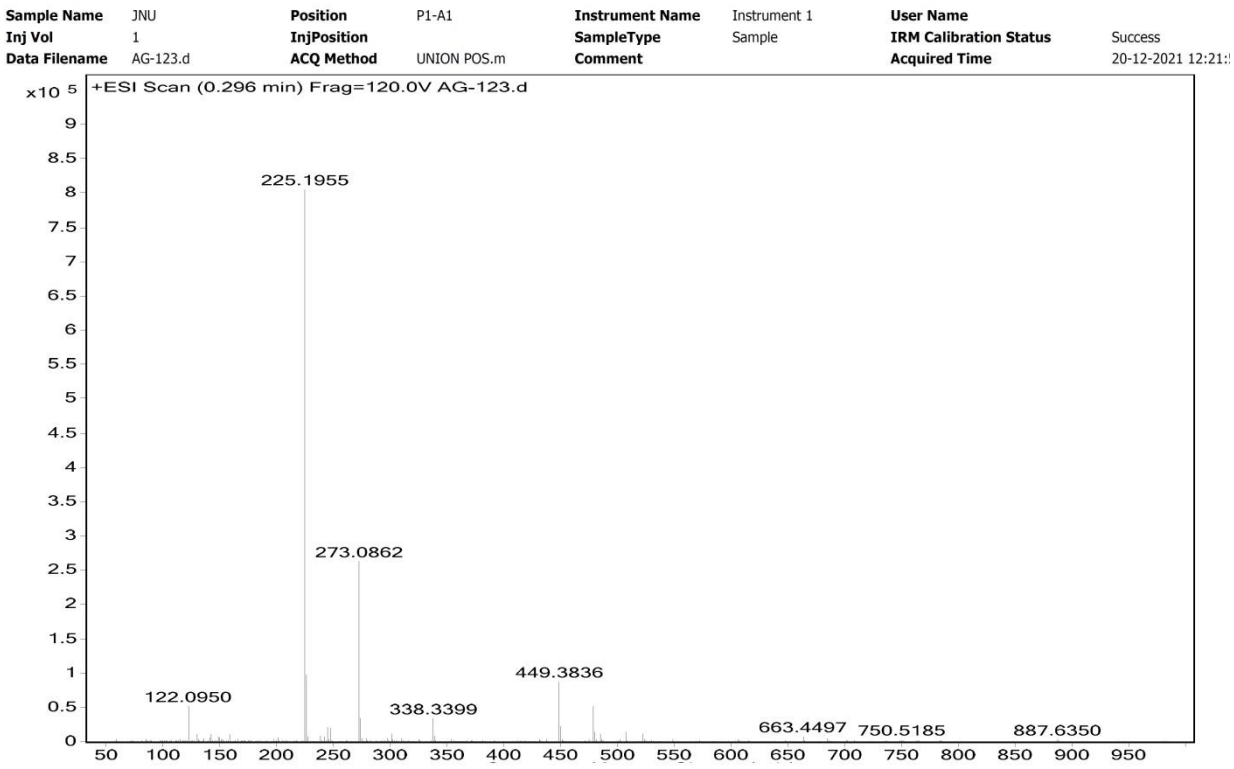

Figure S15 ESI-HRMS of compound **2** in DCM/MeOH showing the peak at 273.0862 (*m/z*) assignable to $[M+H]^+$ at 298K.

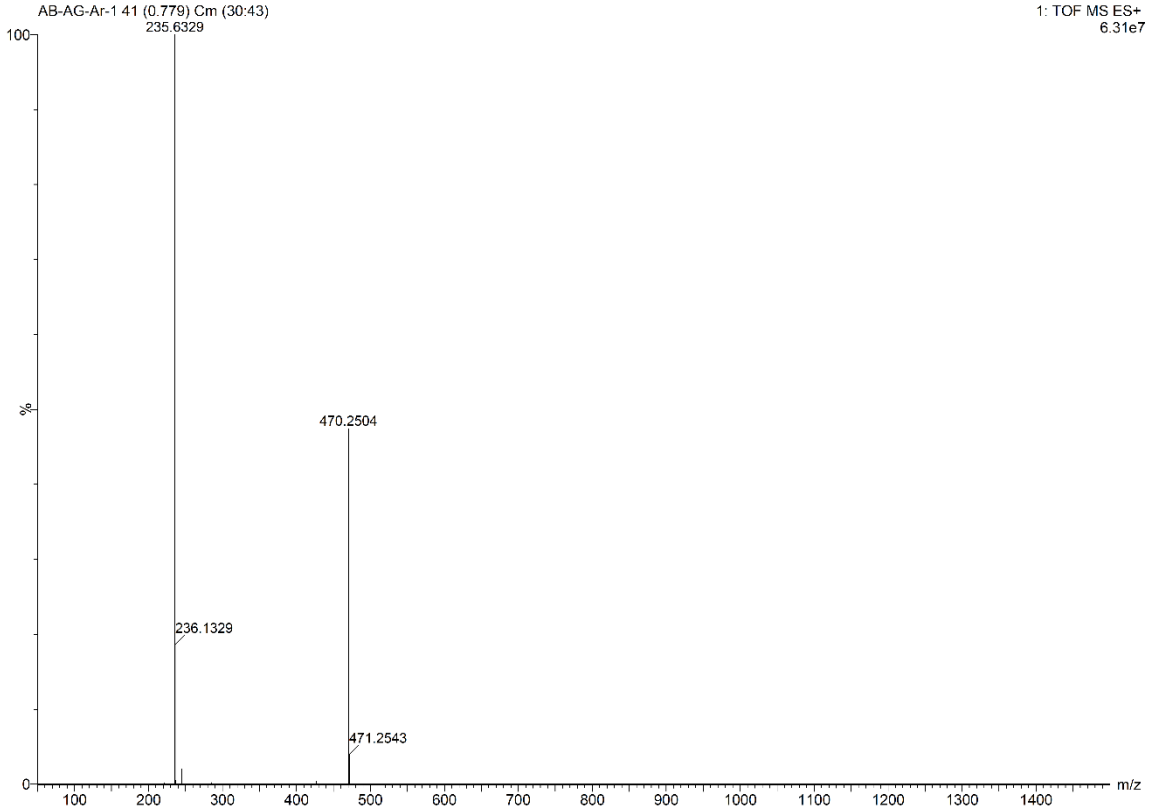

Figure S16 ESI-HRMS of compound **L** in DCM/MeOH showing the peak at 470.2504 (m/z) assignable to $[M]^+$ at 298K.

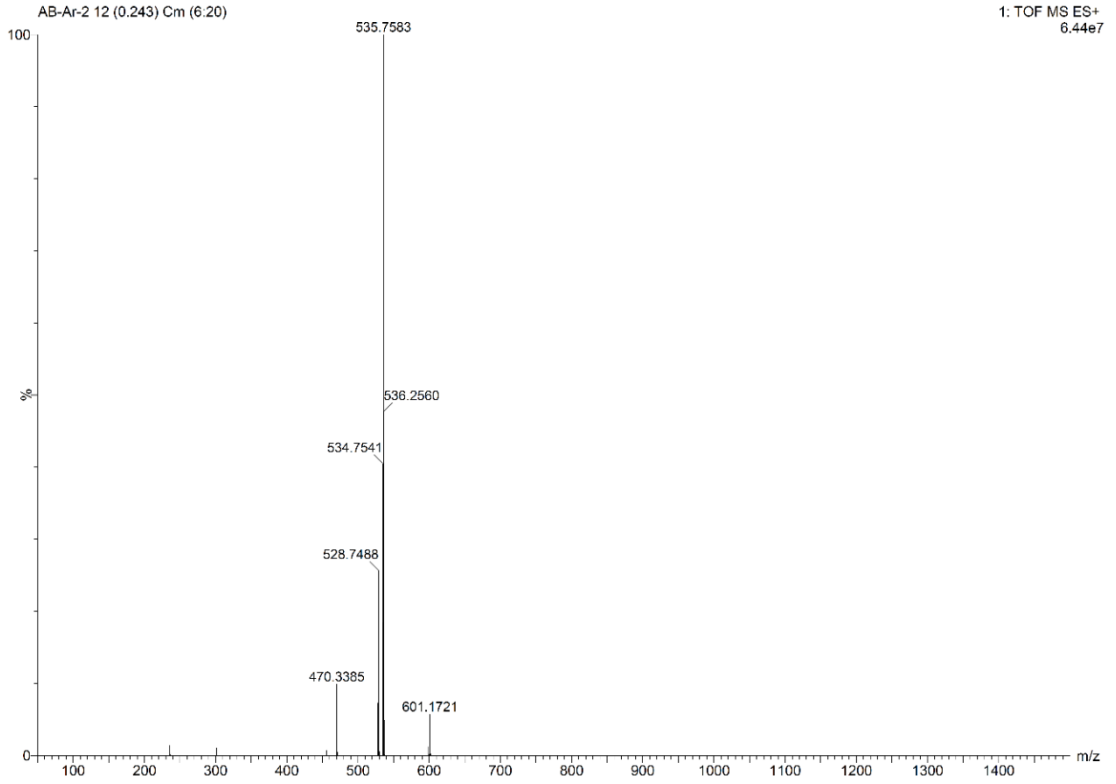

Figure S17 ESI-HRMS of **Ir1** in DCM/MeOH showing the peak at 535.7583 (*m/z*) assignable to $[M]^{2+}$ at 298K.

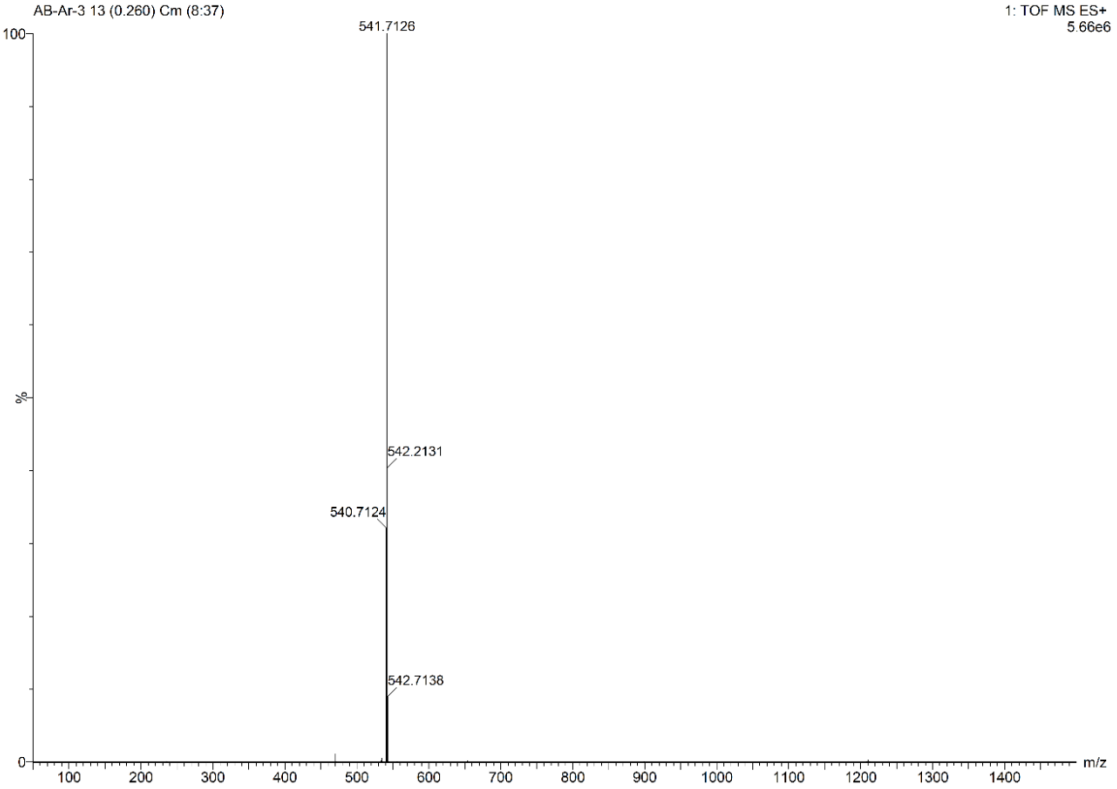

Figure S18 ESI-HRMS of **Ir2** in DCM/MeOH showing the peak at 541.7126 (*m/z*) assignable to $[M]^{2+}$ at 298K.

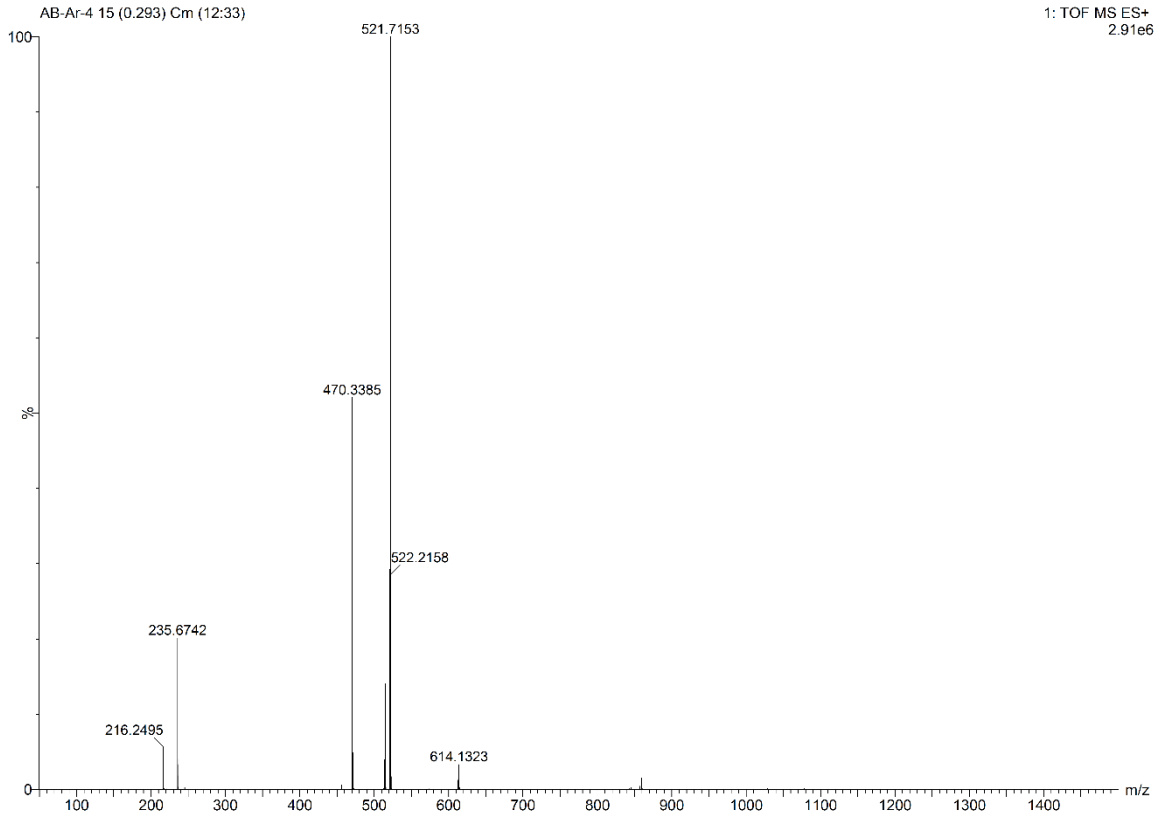

Figure S19 ESI-HRMS of **Ir3** in DCM/MeOH showing the peak at 521.7153 (*m/z*) assignable to $[M]^{2+}$ at 298K.

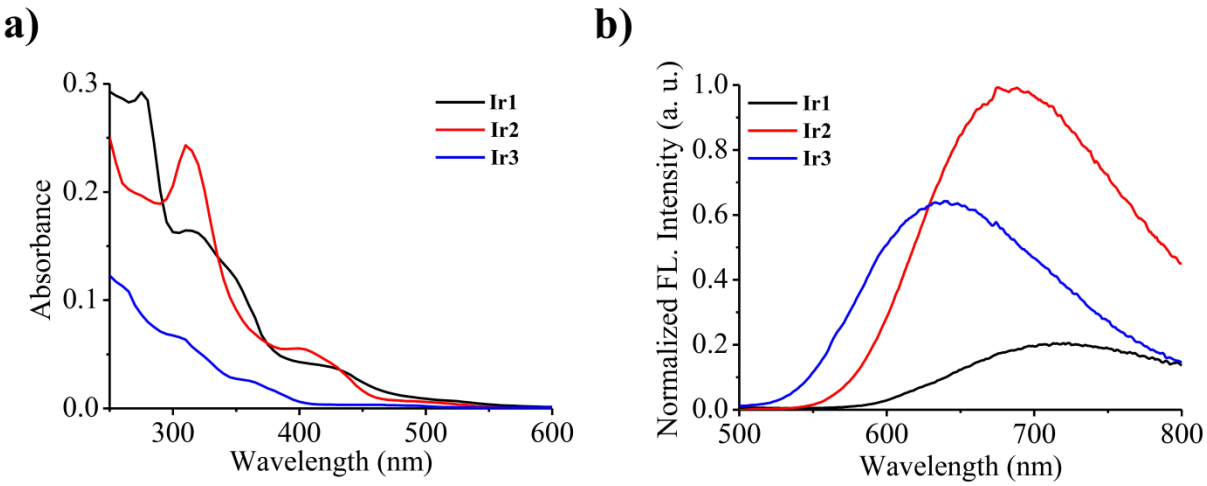

Figure S20 (a) Absorption (10 μM) and (b) normalized emission (50 μM) spectra of the complexes (**Ir1-Ir3**) were recorded in water containing 1% DMSO at RT. The emission spectra were measured upon excitation at 425 nm.

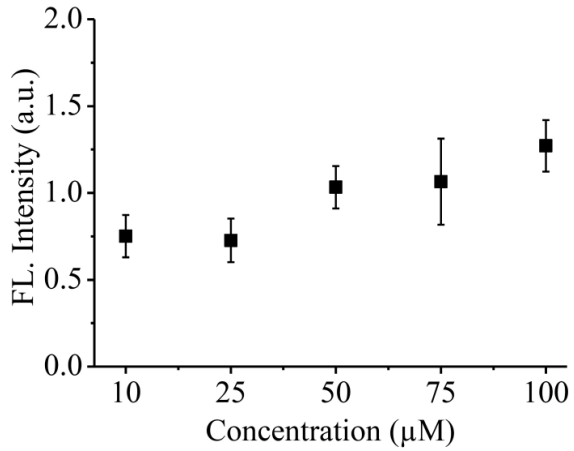

Figure S21 Emission intensity (λ_{ex} = 425 nm, λ_{em} = 720 nm) of complex **Ir1** as a function of concentration.

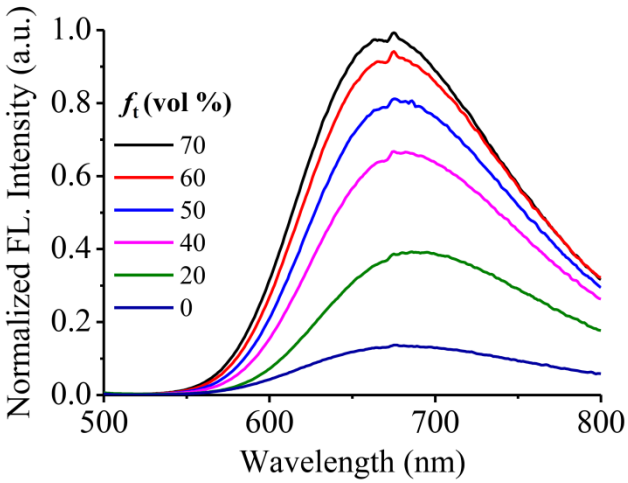

Figure S22 Emission spectra of **Ir2** (50 μM) recorded in a water-THF mixture with different THF fractions (f_t).

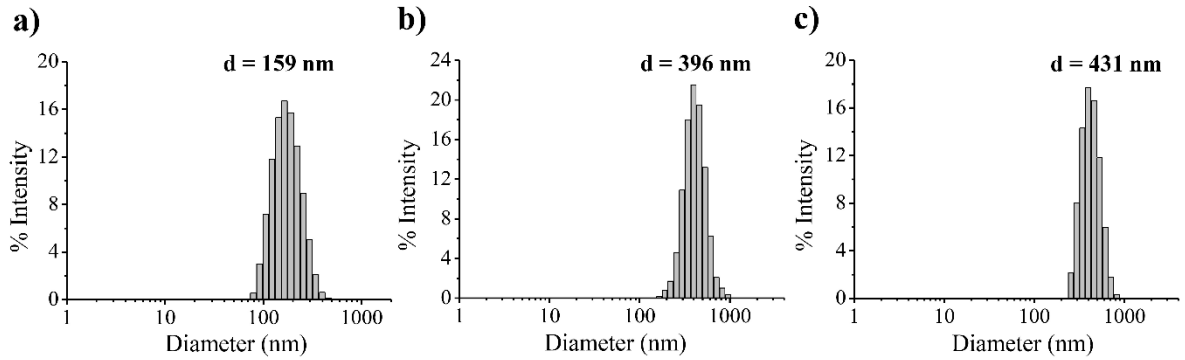

Figure S23 Hydrodynamic diameter (d) and particle size distribution of the complex **Ir1** (50 μM) in the absence (a) and in the presence of 25% THF (b) and 50% THF (c) in a water-THF mixture.

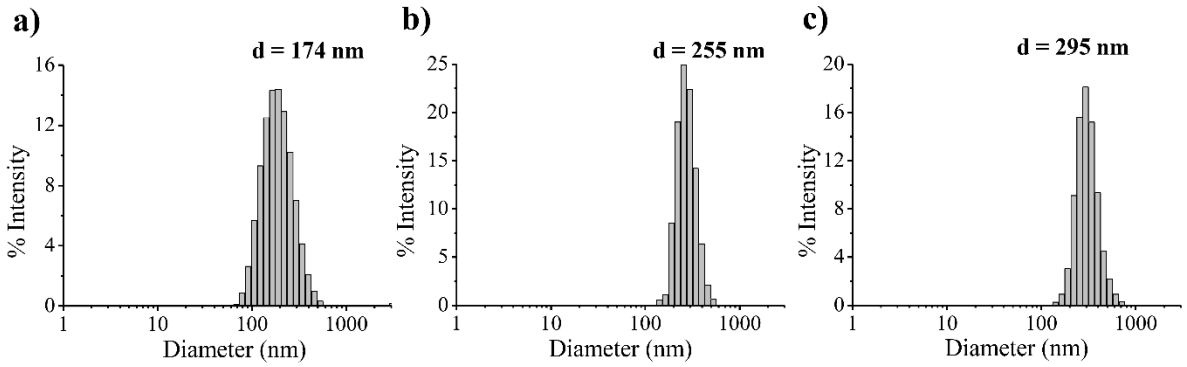

Figure S24 Hydrodynamic diameter (d) and particle size distribution of the complex **Ir2** (50 μM) in the absence (a) and in the presence of 25% THF (b) and 50% THF (c) in a water-THF mixture.

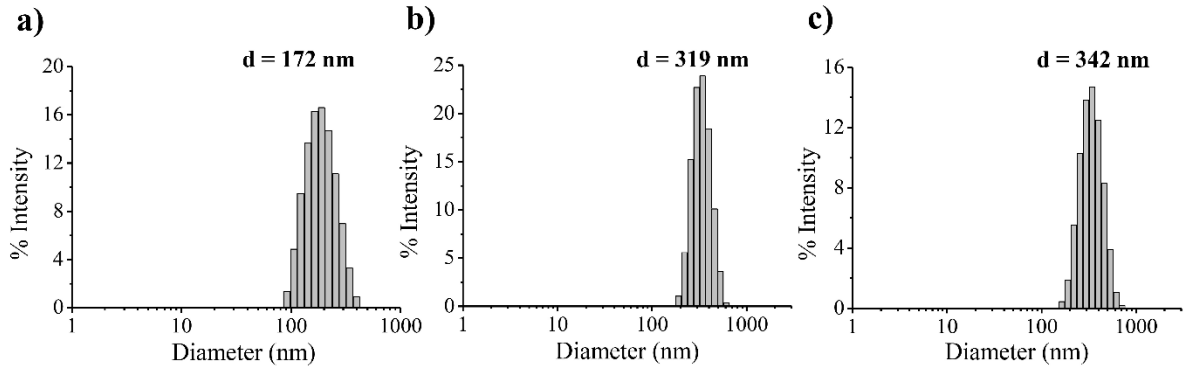

Figure S25 Hydrodynamic diameter (d) and particle size distribution of the complex **Ir3** (50 μM) in the absence (a) and in the presence of 25% THF (b) and 50% THF (c) in a water-THF mixture.

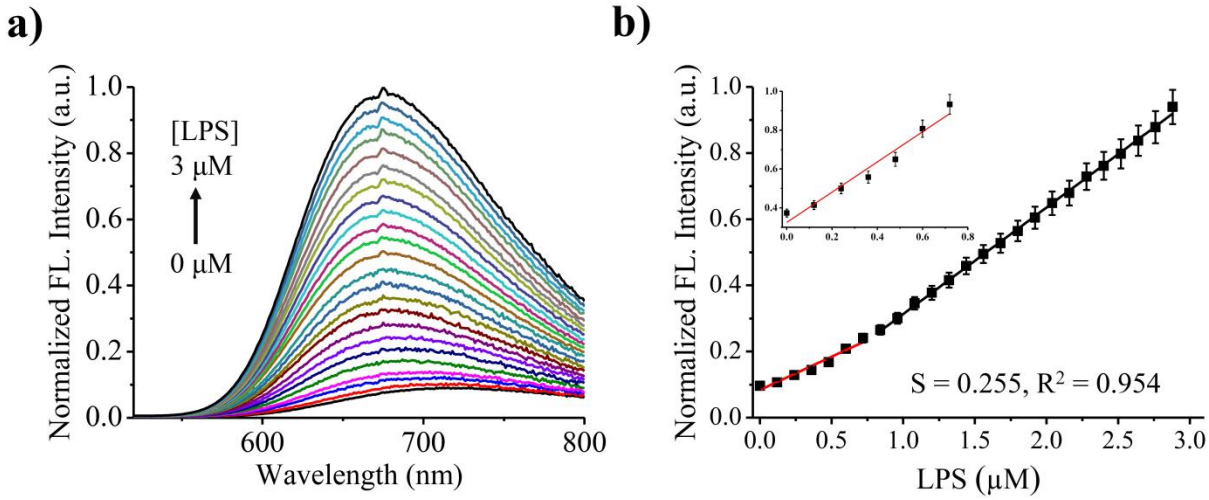

Figure S26 (a) The emission titration spectra of complex **Ir1** (50 μM) upon gradual addition of LPS (0-3 μM). (b) The plot of emission intensity of **Ir1** at 720 nm as a function of the concentration of LPS (0-3 μM). (Inset) The plot and linear fitting of the emission intensity of **Ir1** at 720 nm with different concentrations of LPS (0 to 0.84 μM).

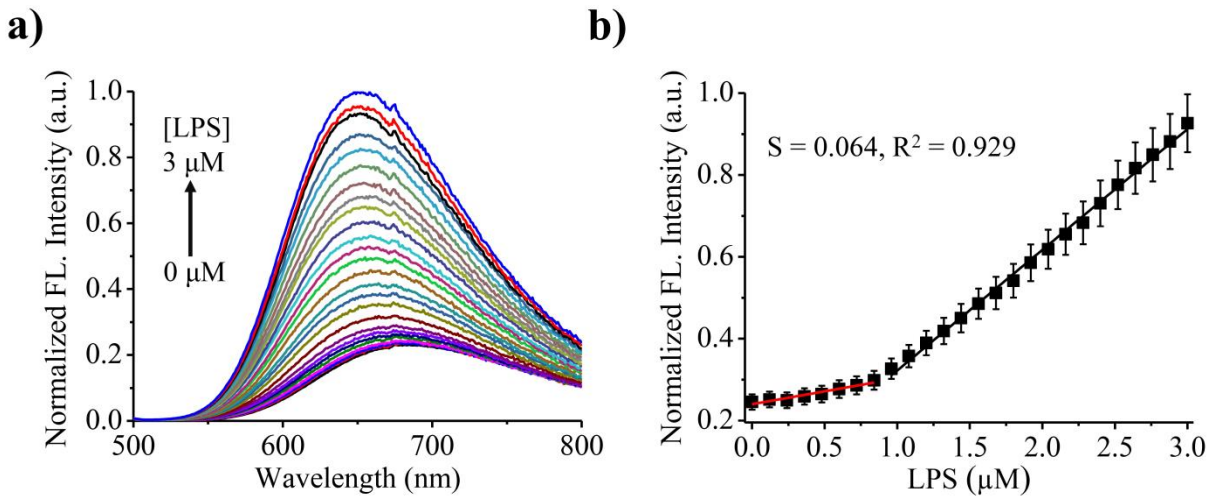

Figure S27 (a) The emission titration spectra of complex **Ir2** (50 μM) upon gradual addition of LPS (0-3 μM). (b) The plot of emission intensity of **Ir2** at 688 nm as a function of LPS showing a linear dynamic range between 0 to 0.84 μM.

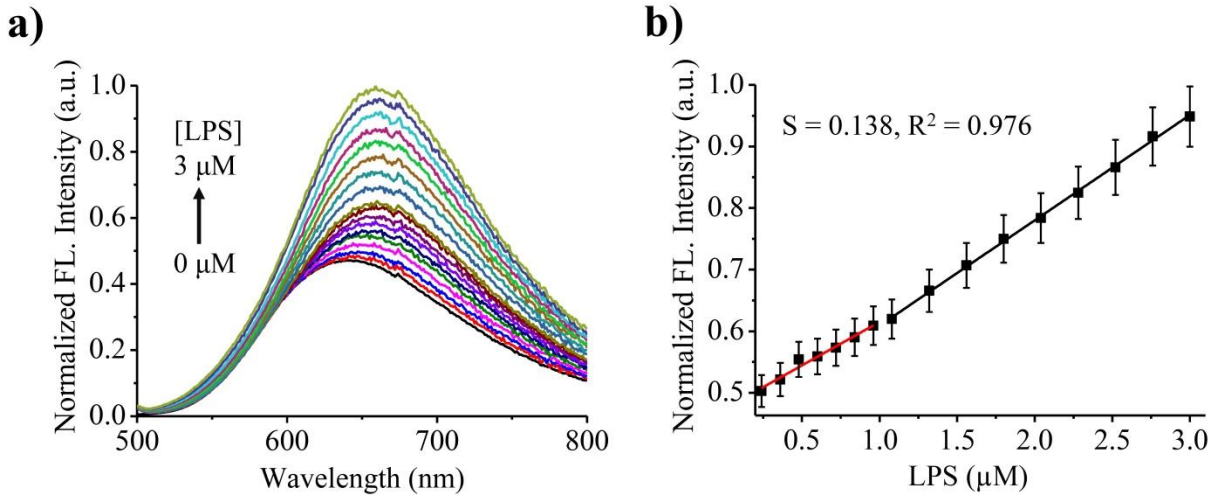

Figure S28 (a) The emission titration spectra of complex **Ir3** (50 μM) upon gradual addition of LPS (0-3 μM). (b) The plot of emission intensity of **Ir3** at 640 nm as a function of LPS showing a linear dynamic range between 0 to 0.96 μM.

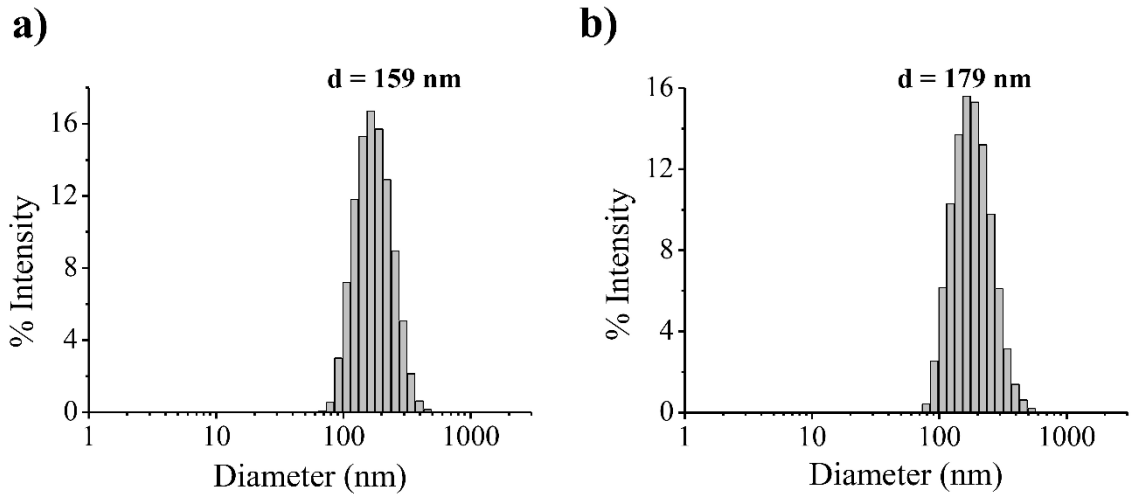

Figure S29 Hydrodynamic diameter (d) and particle size distribution of **Ir1** (50 μM) in aqueous media in the (a) absence and (b) presence of LPS (3 μM).

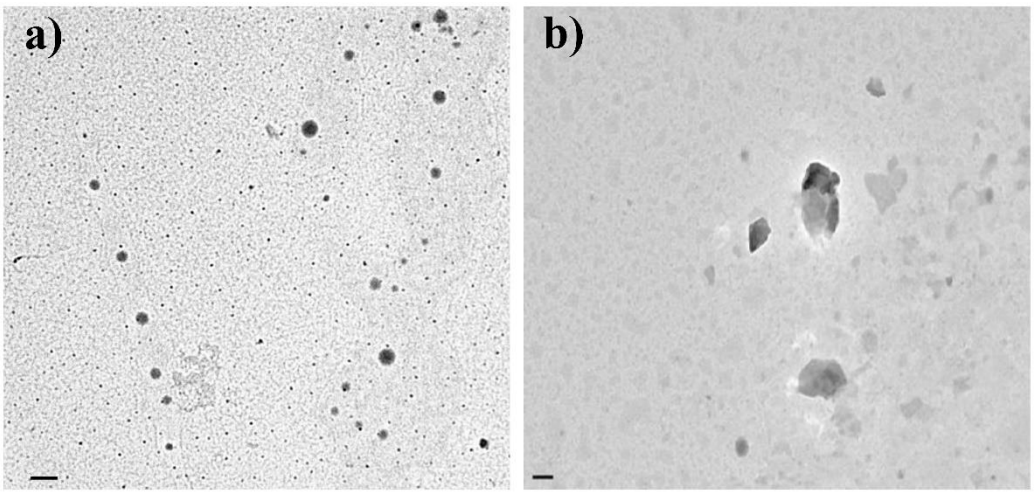

Figure S30 TEM images of complex **Ir1** (50 μM) in water containing 1% MeCN in the (a) absence and (b) presence of 3 μM LPS. Scale bar: 100 nm.

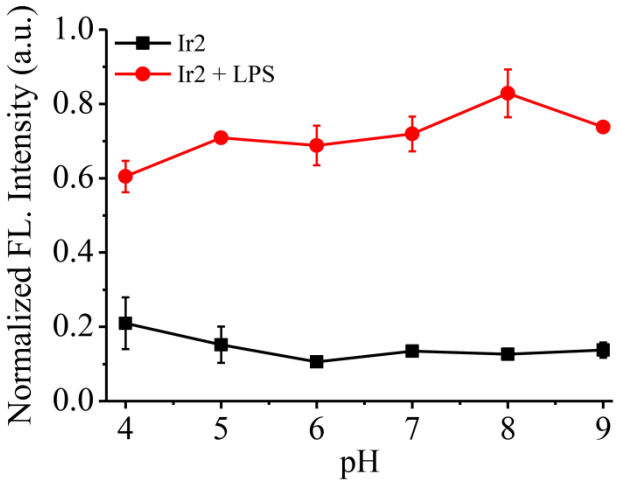

Figure S31 The emission intensity of **Ir2** (50 μM) at 688 nm in 10 mM HEPES buffer in the absence (■) and presence (●) of LPS (6 μM) in different pH solutions at room temperature.

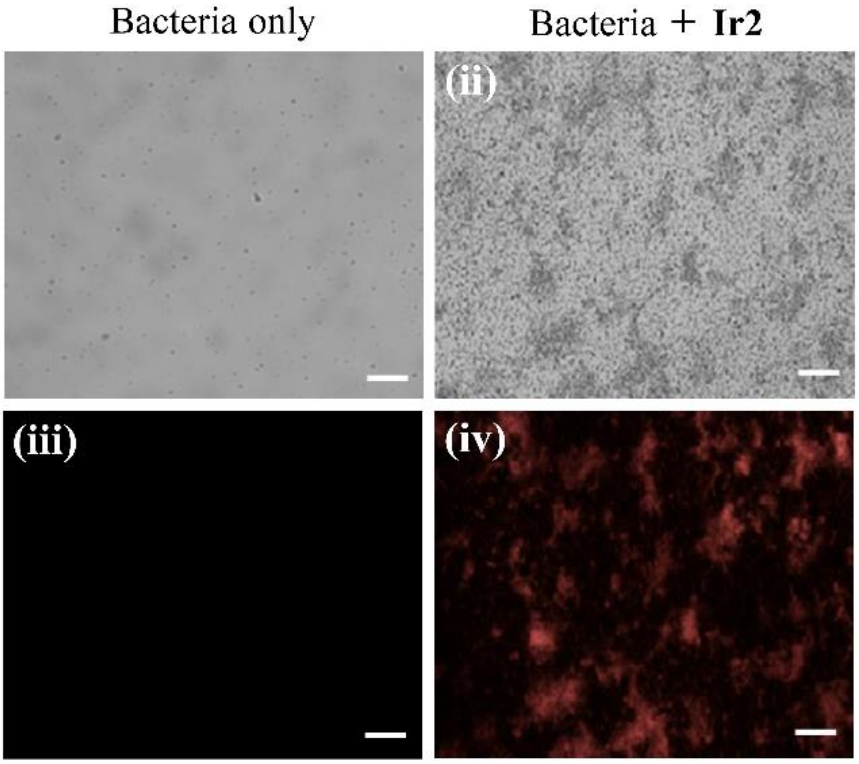

Figure S32 Optical microscopy images of *E. coli* (10^8 CFU/mL) after incubation with 400 μM of complex **Ir2** and the results were observed in complementary bright-field (i,ii) and fluorescence (iii,iv) modes (λ_{ex} = 450-480 nm). Here, left panels (i,iii) indicate results for bacteria only and right panels (ii,iv) for bacteria treated with complex **Ir2**. Scale bar: 5 μm.